International Journal of Signal Processing, Image Processing and Pattern Recognition
Vol.9, No.7 (2016), pp.49-64
http://dx.doi.org/10.14257/ijsip.2016.9.7.06

A New Inspection Method for Bridge Deformation

Bo Cai[1,2*], Zhigui Liu[1], Junbo Wang[1] and Yuyu Zhu[1]

[1]*Southwest University of Science & Technology, Mianyang Sichuan 621010, China*
[2]*China Academy of Engineering Physics, Mianyang, Sichuan 621000, China*
caibo_bupt@126.com

Abstract

The deformation of the location of structural systems is an important step to predict the performance of the system under different conditions. In bridges, the plastic deformations generally occur over a long-span beam after years of service. To improve the detection accuracy and stability of bridge deformation, in this paper, we proposed a new deformation inspecting framework. The total procedure of our algorithm may be concluded as the following three aspects. Firstly, because of the beams of bridges are very long, to improve the resolution of images, we divided the acquiring of the bridge beam image into a sequential images. Secondly, the sequential images are proposed with character point extraction, image stitching, image segmentation, and the calculation of the bridge deformation. Finally, the calculated deformation was compared with the experimental results. According to the experiments on the real bridges and the simulating model, the results indicated that our algorithm may improve the detection accurate to a large extent. At the same time, the proposed algorithm is more flexible than the former proposed algorithms.

Keywords*: Bridge detection; Beam deformation; Image mosaic; Image segmentation; Sequential images*

1. Introduction

The research aims to record and analyze plastic deformation in bridge structure through an investigation of actual beam behavior in large-scale tests of bridge systems subjected to multiple excitations. In order to evaluate the behavior of plastic deformation of the bridge beam, an image sequential based method was used to remotely track deformations of the concrete bridge side surface. Photogrammetry and close-range photogrammetry [1-2] are non-invasive technique of remote visualization of the target components and a computer rendering of the deformation. The tracked deformation of the beam, which discrete points on the column surface along the testing regions, was reduced using a computer program to obtain the lateral displacements of the points and to calculate the vertical and cross-sectional deformation between these points. Close-range photogrammetry [2] has been used for determining the 3D geometry and deformation of bridges since the 1970s. Unfortunately, this technique has not been feasible for wide engineering applications until the 1990s when digital image acquisition and computer processing systems became commercially available. There are many unique advantages of close-range photogrammetry for bridge deformation measurement; for example, it can measure difficult-to-access bridges by taking pictures away from the bridge and record a large amount of 3D information in a short time. A basic bridge photogrammetric measurement system consists of a camera and accessories, targets,

*Corresponding Author

ISSN: 2005-4254 IJSIP

scale bars, and software for photogrammetric processing. Other supplemental instruments, such as a total station or level, may also be used for setting up a coordinate system and checking measurement accuracy.

A thorough literature review on the application of close-range photogrammetry in bridge engineering was mad by the authors and the results were published in a separate paper [3]. Although the systems have been improved steadily, there is still not a turn-key system available to bridge engineers, nor a clear technical guidance for engineers to use. In order to provide engineers with a feasible bridge photogrammetric measurement system, five critical components of the system are addressed in this paper: camera selection and settings; the method of the image acquiring; network control, such as reference system and scale; the processing of the image sequential; and the extraction of the deformation data. Unlike the traditional photogrammetric detection algorithm, in this paper, we modeled the bridge deformation as the deck beam, as shown in Figure 1. Based on this model we aimed at the detection of the relative deformation of the bridge beam, and then reconstruction the total deformation according to the coordinate system of the reference scale bar.

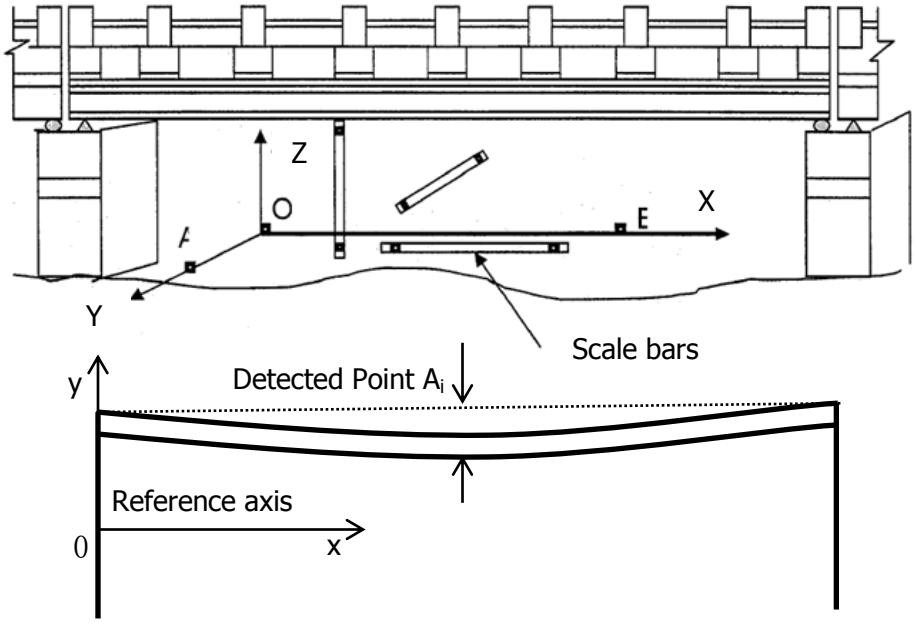

Figure 1. The Model of Our Testing System

This paper presents an automated method for the large-scale concrete bridge beam captured in sequential close-range images taken for the purpose of deformation detection and assessment. When the sequential images have been acquired, we use the image stitching [4-6] algorithm to calculate the transform matrix of each image pair. The transform matrix is just the relationship of the image pair with different view point. When all the transform matrixes have been calculated, we segment beam region of all the sequential images captured from the first step. Following the segmentation procedure is the calculating and extracting of the center points along the reference direction of the beam in each segmented regions. To realize the re-construction of the bridge deformation, we use the reference scale bars as the standard size and coordinate system to extract and calculate the absolute deformation. Generally, the proposed algorithm may be summarized as:

(1) Due to the information of bridge beam deformation are very small, the common single image acquiring method of directly taking the total bridge beams is very difficult to acquire the local deformation because of low resolution of large-

scale objects. The close-range sequential image acquiring method may improve the resolution to a large extent, and at the same time, it may also avoid the influencing of the complicated background.

(2) Unlike the photogrammetric algorithm directly calculating the 3D data of the detected object, we use the correlation of the image pair to calculate the value referenced to the scale bars of the scene. After the related data have been calculated, we exchange the data according to the reference scale bars.

(3) To deal with the large data of the close-range sequential images, the total procedure include image matching, image mosaicking, image segmentation, key point extraction, and the calculation of the bridge deck deformation. For the purpose of improving the detection accuracy of the total deformation, some adjustments have been used in our processing procedure. The experimental results on the simulation condition and the real bridge images show that the total detection frame is adaptable in large scale object detection.

The remainder of this paper is organized as follows. In Section 2, we give the briefly introduction and analysis of the related techniques. The proposed framework is introduced in Section 3.The experimental of each step, such as the image acquisition, the segmentation and mosaic of the sequential images, and the merge of the total information, are introduced in Section 4. In Section 5, the extraction and measurement of the deformation has been introduced. Section 6 is the comparison of our model with experimental image detection results. We go on analyzing the results on simulating condition and the real bridges. Finally, the conclusion and limitations of our model have been discussed in Section 7.

2. Related Work

2.1. The Methods of Bridge Inspection

Researchers have proposed many methods regarding the aim of automated bridge inspection, most of which focus on as-built bridge data collection and defect detection. Laser scanning and photogrammetry are two remote sensing techniques recently used to collect bridge as-built data. Laser scanning can create accurate and detailed 3D range images. Most laser scanners used in construction adopt the time-of-flight principle. Other scanners adopting triangulation of structured-light are seldom applied for scanning large structures due to their limited scanning range of meters and/or safety constraints [7-10]. As for defect detection, many methods have been created to locate cracks in images. they use image processing techniques, such as wavelet transforms and segmentation [11], to extract crack points from the image background [12]. For the purpose of detecting the long and large distance crack, Li, Gang *etc.* [13] use the focal lens to acquire the crack image, according to the calibration of the camera parameters, they detected the crack information with accuracy about 0.05mm.

Seldom paper directly aimed at the detection of the bridge beam deformation. Aimed at the detecting of the dynamic characters of bridge hinging regions deformation, Alemdar, *etc.* [1] proposed a photogrammetric based analysis method to evaluate the deformations of a bridge column surface in plastic hinging locations during the response to strong ground motion. In [14], Pan, Bing, *etc.* described an easy-to-implement yet effective monochromatic light illuminated active imaging DIC (digital image correlation) method for obtaining high-quality images suitable for high fidelity deformation measurement. To realize the measurement of large deformation, Zhengzong Zhang, *etc.* [15] have been given the analysis of a series of deformation images according to the correlation between different images. In [16], Zhenzhong Xiao, *etc.* used the photogrammetric algorithm to measure the large field-of-view deformation. In the paper, they tested a load carrying tower deformation and achieved the accuracy of 0.1mm/m. Using image analysis

algorithm, Lopez, Mauricio, *etc.*[17] given the study of elastic and time-dependent deformations in high performance lightweight concrete. Although there are less study in measurement of bridge beam deformation, the techniques such as, image sequential method in the processing of the large scale object, image correlation, and mosaicking algorithm, are very useful in the detection of bridge beam deformation.

2.2. Image Mosaicking

Image mosaicking as an effective algorithm in dealing with the large scene or object, have been studied for many years. Commonly, the mosaic of image pairs consist three steps: (1) the extraction of the image character points; (2) the matching of the character points; (3) the alignment of the image pixels. In the first step, the character points are often considered as the Harris corners, SIFT [18-21] points, and high-gradient points *etc.* The Harris [22, 23] detector measures the local variation by shifting in various orientations, which is convoluting the original image with a Gaussian kernel. Given the input image I , the convolution of the input image is defined as:

$$S(x,y)=G(x,y)*I(x,y) \tag{1}$$

$$\begin{aligned} G_x(x,y)&=\frac{-x}{2\pi}\exp\left(-\frac{x^2+y^2}{2}\right)\\ G_y(x,y)&=\frac{-y}{2\pi}\exp\left(-\frac{x^2+y^2}{2}\right) \end{aligned} \tag{2}$$

where $G(x,y)$ is the Gaussian kernel function, $G_x(x,y)$ and $G_y(x,y)$ are the two directions, horizontal and vertical ones. In our paper, we use the smoothing window of 7×7 in eq.(1) and (2) to represent the positions of every pixel in the window. Therefore, two kernels G_x and G_y focusing on two orientations are formed. Then, $I_x(x,y)$ and $I_y(x,y)$ of the directional kernels convolution may be calculated.

After every convolution, we have a T calculated as follows:

$$T(A)=Det(A)-\varepsilon Tr^2(A) \tag{3}$$

where A is matrix composed of four elements

$$A=\begin{pmatrix} a_{xx} & a_{xy}\\ a_{xy} & a_{yy}\end{pmatrix} \tag{4}$$

and a_{xx} is the summary of all the $I_x^2(x_i,y_i)$, belonging to the smoothing window. Here a_{xy} is the total value of all the $I_x(x,y)I_y(x,y)$, and accordingly, a_{yy} is the sum of $I_y^2(x,y)$.

Comparing to the Harris corner detector, the magnitude of image gradient, directional gradient of each pixels, and local maximum difference may also be considered as the characters. The magnitude of the image gradient $M_g(x,y)$ and $M_d(x,y)$ may be defined as:

$$M_g(x,y)=\sqrt{G_x^2(x,y)+G_y^2(x,y)} \tag{5}$$

$$M_d(x,y) = \max\left\{\left|G_x(x,y)\right|, \left|G_y(x,y)\right|\right\} \quad (6)$$

where $G_x(x,y)$ and $G_y(x,y)$ is the directional gradient of the image pixel in x-direction and y-direction. For the purpose of extracting the local maximum difference points, we use the local minimum template of 3×3 or 5×5 filter T_L to processing the image, and then using the rough image to deduce it. The extraction of the local maximum point is based on the deduced result. Given an input image I, the local maximum difference is defined as Equation 7.

$$I_{LM} = I - I * T_L \quad (7)$$

where T_L is the minimum filter, when the template size is 3×3, the calculated value of the template is $z_{i,j} = \min\left\{I_{k,l}, k = i-1, i, i+1; l = j-1, j, j+1\right\}$.

In all of the above mentioned character extraction algorithms, the local maximum difference algorithm is the simplest and less time-consuming. In the following character extraction procedure, we use it as the character extraction algorithm. In character point extraction procedure, the number and distribution of character points are the main problems. Basically, the character points should match the following three conditions before the matching procedure.

(1) The character points should be uniformly distributed in the image, when there is any overlapped information of the image pair.

(2) The feature of the extracted points should be consistence to the global condition, instead of the local condition.

(3) To make the RANSAC processing effective and stable, the number *N* of the character points should be fixed or within a range.

Along with the above mentioned standards, we adjust the character point extraction algorithm. Firstly, we calculate the feature value of the image according to Equation (7). The second step is to decide the character number N. Commonly, the choosing of the character points is use a pre-decided threshold, when the threshold is higher, the detected number may be less, otherwise, the detected points may become much more. Both of the two conditions may leads to the matching procedure unstable. Considering of the strength and distribution of the image character points, we choose the maximum value of the image step by step, and after the extraction of the current maximum points, we eliminate the current points and its local (such as 5×5) adjacent points. Under this condition, we may set the number of character points previously, for example 400.

For the purpose of improving the mosaicking efficiency and stability, Jun-Wei Hsieh, *etc.* [24] use the edge pixel as the pre-matching procedure, and then use the character pixel to optimize the total matching of the input pair of images. In [25], the authors use the SVM to estimate the matching and mosaic results, but, the input training images and the evaluation of the parameters is very difficult. For the purpose of improving the traditional method based on characteristic, Gang Xu, *etc.* [26] use the granular computing algorithm to detect the image character points. Aimed at obtain the topology information, Armagan Elibol, *etc.* [27] use the this information to improve the robust of their matching procedure. For the purpose of measure the different descriptors of shape, color, and size in image mosaic, Zoe Falomir [28] give a comparative analysis of different descriptors. All the above mentioned papers are aimed at improving the stability and accurate of image mosaic algorithm before the matching procedure. Aimed at improving the constraint condition, many papers have been given the study of matching based on different constraints, such as, the Delaunay triangulation and affine invariant geometric constraint [29], the template matching with arctangent Hausdorff distance measure [30], the coloring based approach for matching [31], the fast and scalable approximate spectral graph

matching [32], the optimized hierarchical block matching [33], and improved robust algorithm for feature point matching [34] *etc.*

Given two images $\mathrm{I_m}$ and $\mathrm{I_n}$, let $p=(x,y)^T$ be a pixel location in $\mathrm{I_m}$, and $q=(x',y')^T$ be the transformed location in $\mathrm{I_n}$. The affine model is mathematically expressed as:

$$\begin{pmatrix} x' \\ y' \\ 1 \end{pmatrix} = M * \begin{pmatrix} x \\ y \\ 1 \end{pmatrix} \tag{8}$$

where $M=\begin{pmatrix} m_0 & m_1 & m_2 \\ m_3 & m_4 & m_5 \\ m_6 & m_7 & m_8 \end{pmatrix}$. The technique used to estimate M is random sample consensus (RANSAC) [35]. In the case, we may choose the matched feature points pairs to evaluate M using the direct linear transformation (DLT) method. Unfortunately, when the input pairs of character points extracted from the first step are redundancy, this algorithm may leads to local minimum.

2.3. Image Segmentation

For the purpose of acquiring the deformation data, the segmentation of the beam region is also an important step. Active Contour Model (ACM) based segmentation algorithms [36-40] have been widely investigated and applied to the image segmentation. Comparing to the other ACM based models, the Local Binary Fitting [41] (LBF) model is more adaptive to the local and global information of the different input images. In this step, we choose the adjusted LBF model as the basic segmentation algorithm.

Given the input image $I(x)$ on the image domain R, LBF model use the region-based intensity information as a controllable scale in the energy model.

$$\begin{aligned} &E^{LBF}\left(C, f_1(x), f_2(x)\right) \\ &= \int_R E_x\left(C, f_1(x), f_2(x)\right)dx \\ &= \lambda_1 \int_R \left[\int_R g(x-y)\left(I(y)-f_1(x)\right)^2 H\left(\phi(y)\right)dy \right] dx \\ &+ \lambda_2 \int_R \left[\int_R g(x-y)\left(I(y)-f_2(x)\right)^2 \left(1-H\left(\phi(y)\right)\right)dy \right] dx \end{aligned} \tag{9}$$

The nonnegative weighted kernel function $g(x-y)$ is chosen as the Gaussian function $g(u)=\frac{1}{(2\pi)^{n/2}\sigma^n}e^{-|u|^2/2\sigma^2}$. Where $H(\phi)$ and $\delta(\phi)$ are Heaviside function and Dirac function respectively. Generally, the regularized versions are selected as

$$\begin{aligned} &H_\varepsilon(z)=\frac{1}{2}\left(1+\frac{2}{\pi}\arctan\left(\frac{z}{\varepsilon}\right)\right) \\ &\delta_\varepsilon(z)=\frac{1}{\pi}\frac{\varepsilon}{\varepsilon^2+z^2}, \quad z\in R \end{aligned} \tag{10}$$

Keeping $\phi(x)$ fixed, and minimizing the energy $E^{LBF}(\phi, c_1, c_2)$ with respect to the constant $c_1 = f_1(x)$ and $c_2 = f_2(x)$ by using Euler-Lagrange equations. The calculation of c_1 and c_2 may be obtained:

$$\begin{cases} c_1(\phi) = \dfrac{\int_R g(x) * \left[I(x) H(\phi(x)) \right] dx}{\int_R g(x) * H(\phi(x)) dx} \\ c_2(\phi) = \dfrac{\int_R g(x) * \left[I(x) (1 - H(\phi(x))) \right] dx}{\int_R g(x) * (1 - H(\phi(x))) dx} \end{cases} \tag{11}$$

Here, c_1 and c_2 are the weighted means of the foreground and background of the image. The weighted coefficient $g(x-y)$ is used to dispose the local characterization of the image. But the calculation of c_1 and c_2 is based on the evolutionary contour, the more homogeneous the inner region pixels the more quickly the edge would be achieved. And at the same time the edge would be more accuracy. However, when the region is inhomogeneous or transitional, it may cause wrong segmentation, especially on the blurred edges. It's very difficult to decide whether the local segmentation or the global segmentation is right when there is no more information. According to the above analysis, we choose the global contrast as the guide components to punish the inconsistent segmentation of local and global condition in LBF model.

For the purpose of letting global region information guide the iteration, we divide the image into two parts, region inner and edge areas according to the mean gradient of the input image. Before the calculation of the background mean and foreground mean, we use the directional mean value template to resample the region inner pixels of $\phi(x)$. After the resampling processing, we keep c_1' and c_2' fixed, and then to minimize the energy function $E(C, c_1', c_2')$. Parameterizing the descent direction by an artificial time t, we can obtain the corresponding variational level set function.

Keeping the clusters c_1' and c_2' fixed, the level set function is updated by solving the gradient flow equation:

$$\phi^t = \phi^{t-1} - \eta \frac{dE\left(\phi, c_1', c_2'\right)}{d\phi} \tag{12}$$

where η is the time step.

$$\begin{aligned} &\frac{\partial \phi'(x,t)}{\partial t} \\ &= \delta(\phi') \Big[-\lambda_1 \left(I(x) - c_1' \right)^2 + \lambda_2 \left(I(x) - c_2' \right)^2 - \eta_1 \left(I(x) - m_1' \right)^2 \\ &+ \eta_2 \left(I(x) - m_2' \right)^2 \Big] + \delta(\phi') \left[\mu div\left(\frac{\nabla \phi'}{|\nabla \phi'|} \right) - \upsilon \right] \end{aligned} \tag{13}$$

where m_1' and m_2' are the mean of the up and down mean of the gray scale, η_1 and η_2 are the fixed coefficients (In all the following experiments, we choose $\eta_1 = \eta_2 = 0.0001$). When the local difference is smaller than the global difference, the value of $\lambda_i \left(I(y) - c_i' \right)^2 + \eta_i \left(I(y) - m_i' \right)^2$, $i = 1, 2$ is mainly controlled by the global dividing. On the contrary, the dividing is mainly influenced by the local information.

3. The Proposed Model

To realize the detection of the bridge beam deformation based on the sequential images, the developed methodology encompasses structured procedures for image capturing, image character extraction, image mosaic, bean region segmentation, and the extraction of the bridge beam centering points. The common forms of deformation experienced in surface crack deformation, local beam deformation, and the plastic deformation of different regions. In this paper, we aimed at the detection of the plastic deformation of bridge beam.

As have been mentioned above, we acquire the bridge beam images with focal lens camera. Then, we use the image mosaicking algorithm to calculate the correlation matrixes $T_{i,i+1}, i = 1, \ldots N-1$ of all the adjacent sequential images. After the calculation of the sequential images, we segment the bridge beam regions of each image. The segmented regions of sequential images are just the key regions of the bridge beam. For the purpose of avoiding the influence of the local crack regions, we fit the local edges of the segmented result. The next step is the extraction of all the character points of the bridge beam. In this paper, we simply choose the region center of referencing direction as the character points as our testing results. Finally, unlike the photogrammetric testing algorithm which directly calculating the real value of each local region, we calculate the related value of all the extracted points according to the image which contains the reference scale bars, and then, translating all the testing value into real value. Generally, the procedure of our proposed bridge beam deformation detecting framework may be concluded as the following six steps, the block diagram is shown in Figure 2.

(1) Acquiring the sequential images of the concrete bridge beam. In this step, for the purpose of acquiring more detailed deformation, we use the focal lens camera with 4000×6000 pixels to get the local beam image. At the same time, because of our next step is the mosaicking of the adjacent image pair, so the adjacent images should have some parts overlapped. In our experiments, we let the overlapped regions of the adjacent images have about half of the image size.

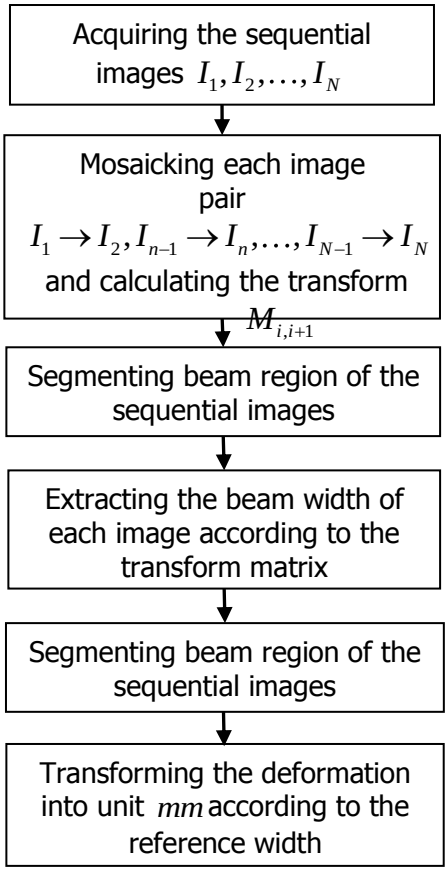

Figure 2. The Proposed Framework of Concrete Bridge Deformation Detection

(2) Mosaicking of each image pair. The main propose of this step is to get the transform matrix $M_{i,i+1}$ between the adjacent images. But, when the image size is larger, the common corner and scale invariable feature transform (SIFT) detectors are very time consuming. In this step, we will give some adjustments of the character detector and the processing of the matching procedure.

(3) Calculating all of the transform matrixes of the image sequence. Commonly, the transform matrix is estimated by using the RANSAC algorithm. The distribution and number of the character points may influence the accurate and efficient to a large extent. In this step, we use the two step matching algorithm to realize the total matching procedure of all sequential images.

(4) Segmenting the beam regions of all the images. As the problem in the second step, when the image size is large, the common iterative algorithms are very time consuming. In this paper, a two steps segmentation algorithm is adopted. In the first step, we resize the input image to a small sized image, and then segment the small image. In the second step, we use the region information of the first step to segment the image into some small blocks which contain the beam regions, the segmentation and combination of the blocks are the total procedure of the large image segmentation.

(5) Extracting the character point of each image. To improve the accuracy of the beam deformation, we extract the character points from each segmented region of the sequential image.

(6) Converting the position into unit *mm* and translate all character points into the coordinate system. When all of the deformation data in the images have been extracted, the exchange of the pixel width into unit *mm* is the last step. In this step,

we choose the reference scale bars of the scene as the transform standard to realize the conversion.

Generally, the detection of the bridge deformation are a complicated procedure, each of the above mentioned step may causing the wrong calculation. In the following section, we will give the detailed introduction of our proposed algorithm to improve the accurate and stability of the total procedure.

3.1. Image Acquisition

To acquire the long bridge beam image information based on the proposed algorithm, the image sequence should have some parts overlapped in adjacent images. At the same time, the view point of all the sequential images should have little difference to keep the testing result more stable and accuracy. So, in this step, we choose the focal lens camera and acquire the images far from the bridge. On this condition, the close-range information and viewpoint conditions may all be satisfied. The acquired images (the image size is 4000×6000) are shown in Figure 3.

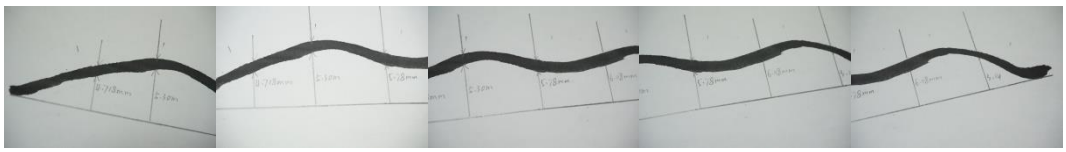

Figure 3. The Acquired Image Sequence

3.2. The Mosaicking of the Sequential Images

To realize the matching of two 4000×6000 images, the directly matching algorithm is very time-consuming. As have been analyzed in the above section, we adopt the two step matching algorithm. In the first step, we resize the large image into 400×600. Then, we extract the local maximum difference points as the character points to pre-match the two images. The matched homograph matrix $M'_{i,i+1}$ of the resized images is used as the constraint of the overlapped region searching. On this condition, we can avoid the calculating of the large total image points. Under this condition, we give the deeply study of the different character points detection algorithms and the matching stability of image mosaic. Comparing to the other algorithms, the main advantages of our method can be highlighted as:

(1) For the purpose of making our algorithm more adaptable to the different contents and size of the processing images, we divided the matching procedure into two steps, the rough and accurate matching procedure.

(2) To avoid the unpredicted character point number under the threshold condition, we give a comparable study of the different character detection algorithms, and proposed a new fixed character point number detecting algorithm.

(3) Unlike the blindly pre-matching constraints extracting, we deal with the constraint condition after the rough matching procedure. It makes the evaluation of the matching result and constraint condition more easily and stable.

(4) Because of the total detecting accurate is influenced by the matching accurate of each image pairs, by adding the edge constraint and pre-matching procedure, our algorithm improved the total efficient and accurate to a large extents. The total procedure of the matching procedure is shown in Figure 4.

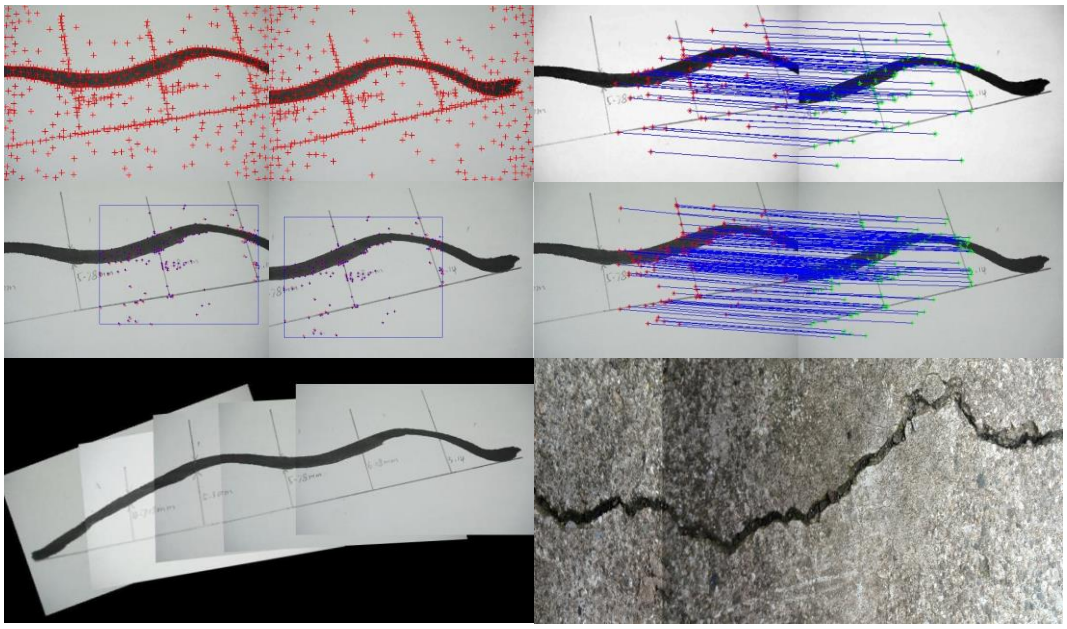

Figure 4. The Procedure of the Sequential Image ma

3.3. Segment of the Beam Regions of the Sequential Image

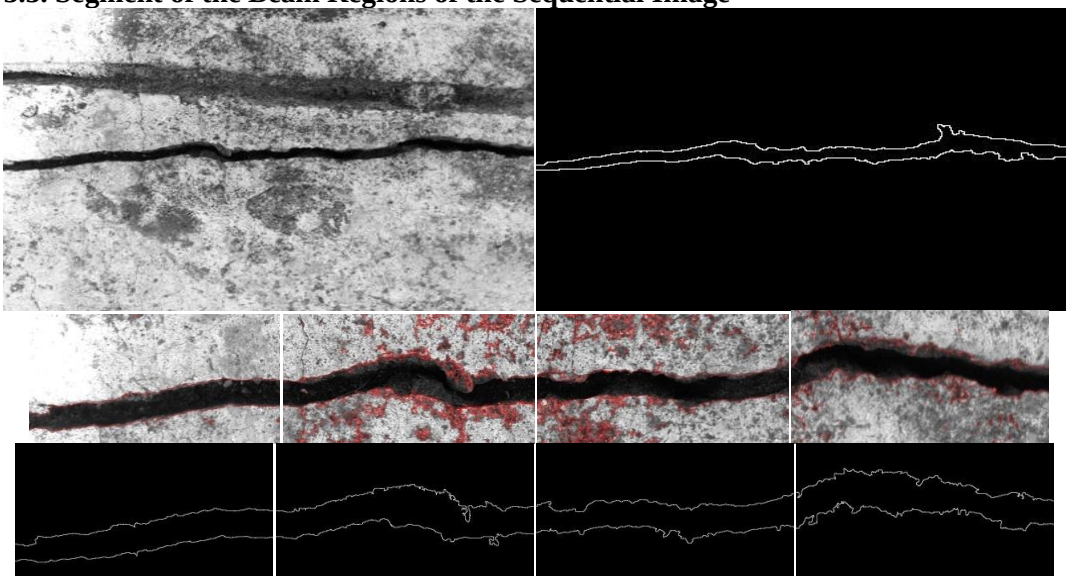

Figure 5. The Segmentation Procedure of One Sequential Image

Because of the LBF model use the iterative algorithm to calculate the minimization segmentation result. When the image size is larger, the processing is also very time-consuming. To improve the efficient of the segmentation procedure, in this paper, we use a three step algorithm to realize the segmentation of the large image. Firstly, we resize the image to a small image, and segment it into beam region and background. Secondly, we choose the local region which contains the beam as the rough segmentation result and divide the local image into some sub-images. Finally, we use the adjusted LBF model to segment the sub-images and extract the beam regions of each sub-image. The combination of all the extracted regions is the total segmentation result of one sequential image. Figure 5 shows the processing of one sequential image.

4. The Extraction and Measurement of the Deformation

After the matching and segmentation have been done, the next step is to extract the beam regions of the sequential image. There are two steps to realize the testing of the beam deformation. The first step is the extracting of the different parts of the beam width from the sequential images. The second step is the conversion of the extracted pixel position reference coordinate system.

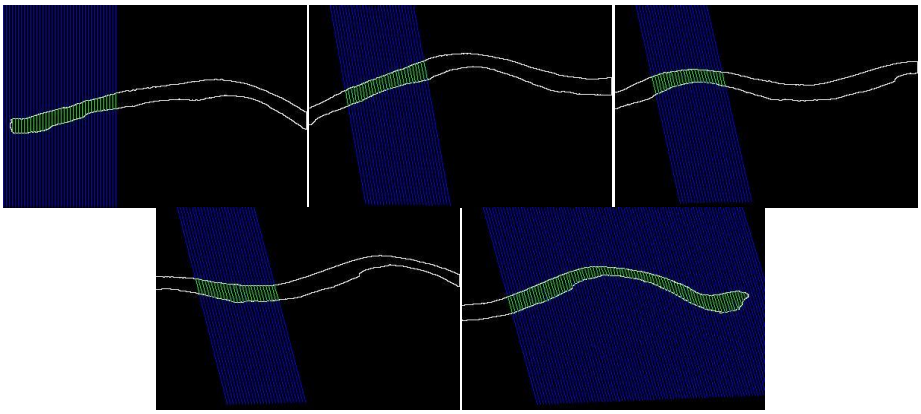

Figure 6. The Extraction of the Crack Width from the Sequential Images.

To realizing the extraction of the different parts of the sequential images, the homogeneous matrixes $T_{i,i+1}$ calculated from the matching procedure are needed to decide the direction and shift value of the sampling line in different images. In the image acquiring procedure, we have not constraint the view point of different local beam images except the overlapped region. So, in this step, the difference should be considered in. Along with the analysis of the above mentioned, we extract the reference bars in the image as the reference coordinate of the total beam.

5. Experimental Results

To evaluate the accurate and efficient of our proposed algorithm, we use the simulated bridge beam images (shown in Figure 4) to verify the effectivity and accuracy of the proposed algorithm. In the experiment, we use Matlab R2012 to implement the image processing algorithm. According to our experiments on the simulating model, the calculated value of the sequential image beam region up to about 400 pixel width with about 7mm, it improved the resolution to a large extents comparing to the single image detection algorithm. For the purpose of realizing the converting of the pixel length to unit mm, we calculate the pixel length of the pre-signed reference scale bar of the image, and use the length ratio to calculate all extracted value. Figure 7 shows the extracted result of image pixel length and the converted result. Along with the sampling line, the difference between the calculated results and the re-tested results is very less. In the reference image, the width of the reference scale bars is 4.718 mm, and the calculated result is about 4.7243 mm. Table 1 shows the calculated result when we choose the third image as the reference value. Except the resolution of the beam width have been improved, the system may also improve the sampling points of the total bridge beam length.

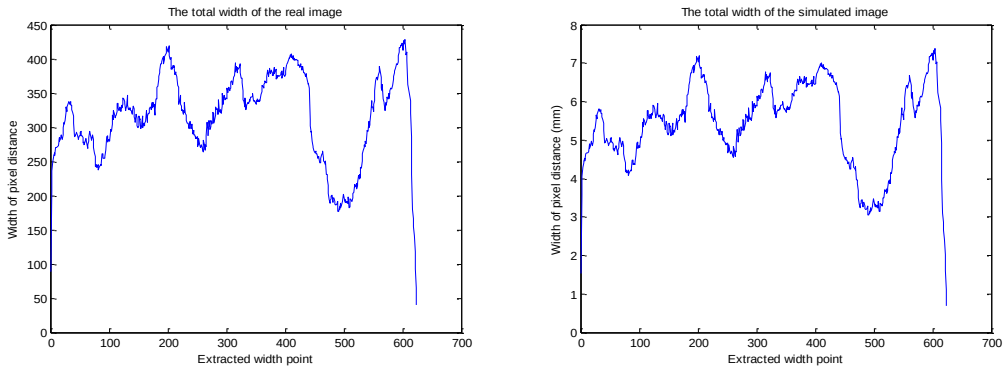

(a) (b)

Figure 7. The Detected Pixel Width and Real Width of the Simulating Image.

Table 1. Comparison of the Measured Width and the Signed Width

Points of images	Calculated results (mm)	tested results (mm)	Mean error (mm)
Image1	4.724 5.305	4.718 5.30	0.005
Image2	4.726 5.307 5.767	4.718 5.30 5.78	0.009
Image3	5.301 5.773 6.072	5.30 5.78 6.08	0.003
Image4	5.745 6.047 3.125	5.78 6.08 3.14	0.027
Image5	6.066 3.118	6.08 3.14	0.018

6. The Experiment of the Real Bridge Beam

In the experiments of the real concrete crack image, because of the crack style and the contamination of the scene, the segmenting results of the real crack image would be influenced. For the purpose getting the correct overlapped sampling line, we chose about 5 covered sampling line and use the mean value of these lines as the converting ratio of different images. The segmenting result, sampling processing and calculated width is show in Figure 8.

7. Conclusion

In this paper, a new crack inspection method of concrete crack has been developed for practical use. The proposed crack inspection method includes three main parts: a specially designed image acquisition way of the concrete crack makes the image detection of the crack more flexible and accuracy. The adjusted image matching algorithm makes the matching processing more stable and accuracy. And at the same time, the segmentation of the concrete image is the most challenging problem in our framework. By adding the local and global information in the evolution of LBF, the segmentation problem becomes more stable in the experiments. The simulating experiments on the image sequence show that the detection results are very accurate comparing to the other algorithms.

In order to improve the inspecting accuracy, the segmentation procedure is very important in the proposed algorithm. Commonly, the more accurate the edge been detected, the more reasonable the detected results would be. In our following study, we will give the deep study of the segmentation algorithm based on different crack condition.

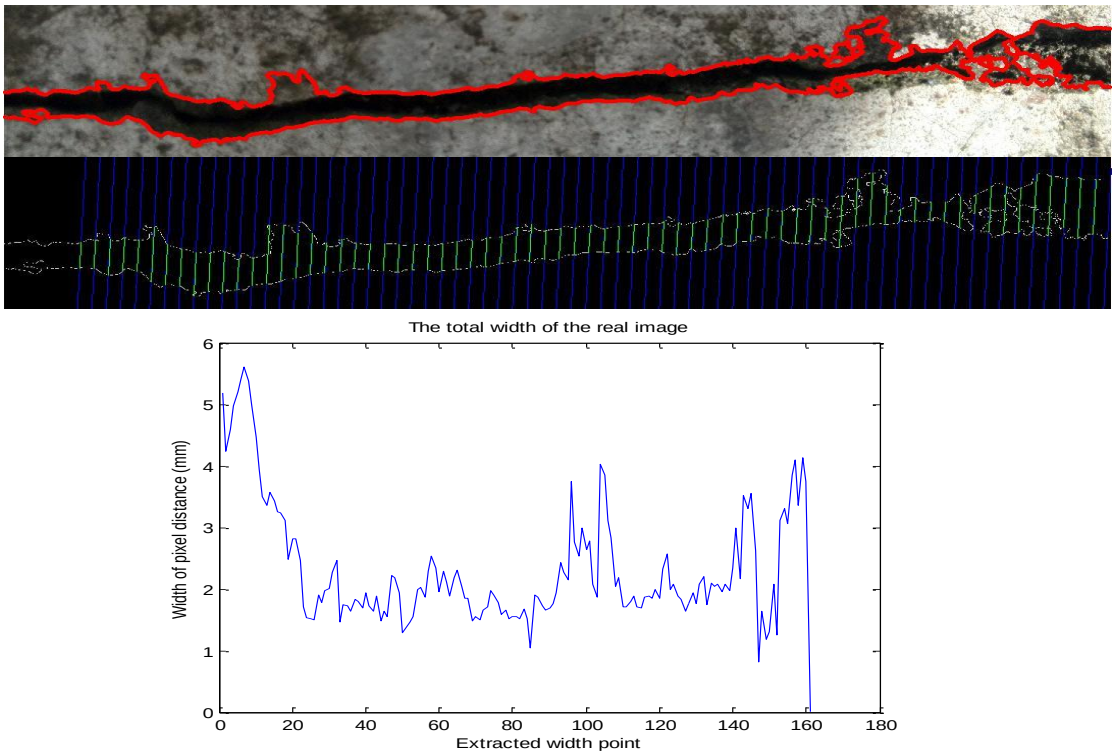

Figure 8. The Results of the Crack Width every 40 Pixels

Acknowledgements

The authors thank the anonymous reviewers for their many valuable comments and suggestions that helped to improve both the technical content and the presentation quality of this paper.

References

[1] Z. F. Alemdar, J. Browning and J. Olafsen, "Photogrammetric measurements of RC bridge column deformations," Engineering Structures, vol. 33, **(2011)**, pp. 2407-2415.
[2] R. Jiang and D. V. Jauregui, "Development of a digital close-range photogrammetric bridge deflection measurement system", Measurement, vol. 43, **(2010)**, pp. 1431-1438.
[3] C. S. Fraser, "Industrial measurement applications, in:Close Range Photogrammetry and Machine Vision: Whittles Publishing, Roseleigh House", Latheronwheel, Caithness, KW5 6DW, Scotland, UK, **(2000)**.
[4] Y. Meng, G. Bao-Long and Z. Xu, "Optimal derivative filters with well-distributed based image mosaic algorithm," presented at the Proceedings of the 30th Chinese Control Conference, Yantai, China, July 22-24, 2011.
[5] H. Wang, X. Liu, S. Zhang and W. Quan, "Novel Image Mosaic Algorithm for Concrete Pavement Surface Image Reconstruction," Procedia - Social and Behavioral Sciences, vol. 96, **(2013)**, pp. 2692-2697.
[6] Y. Wan, D. Wang, J. Xiao, X. Lai and J. Xu, "Automatic determination of seamlines for aerial image mosaicking based on vector roads alone", ISPRS Journal of Photogrammetry and Remote Sensing, vol. 76, **(2013)**, pp. 1-10.
[7] F. D. A. López, C. Ordóñez, J. Roca-Pardiñas and S. García-Cortés, "Point cloud comparison under uncertainty. Application to beam bridge measurement with terrestrial laser scanning", Measurement, vol. 51, **(2014)**, pp. 259-264.
[8] B. Riveiro, H. G. Jorge, M. Varela and D. V. Jauregui, "Validation of terrestrial laser scanning and photogrammetry techniques for the measurement of vertical underclearance and beam geometry in structural inspection of bridges", Measurement, vol. 46, **(2013)**, pp. 784-794.

[9] P. Tang and B. Akinci, "Formalization of workflows for extracting bridge surveying goals from laser-scanned data", Automation in Construction, **(2011)**.
[10] B. Riveiro, P. Morer, P. Arias, and I. D. Arteaga, "Terrestrial laser scanning and limit analysis of masonry arch bridges", Construction and Building Materials, vol. 25, **(2011)**, pp. 1726-1735.
[11] H. Xu, Y. Tian, S. Lin and S. Wang, "Research of image segmentation algorithm applied to concrete bridge cracks", presented at the Third International Conference on Information Science and Technology, Yangzhou, Jiangsu, China, **(2013)**, March 23-25.
[12] R. S. Lim, H. M. La and W. Sheng, "A Robotic Crack Inspection and Mapping System for Bridge Deck Maintenance", Automation Science and Engineering, IEEE Transactions on, vol. 11, **(2014)** April, pp. 367 - 378.
[13] G. Li, S. He, Y. Ju and K. Du, "Long-distance precision inspection method for bridge cracks with image processing", Automation in Construction, vol. 41, **(2014)**, pp. 83-95.
[14] B. Pan, D. Wu and Y. Xia, "An active imaging digital image correlation method for deformation measurement insensitive to ambient light", Optics & Laser Technology, vol. 44, **(2012)**, pp. 204-209.
[15] Z. Tang, J. Liang, Z. Xiao and C. Guo, "Large deformation measurement scheme for 3D digital image correlation method", Optics and Lasers in Engineering, vol. 50, **(2012)**, pp. 122-130.
[16] Z. Xiao, J. Liang D. Yu, and A. Asundi, "Large field-of-view deformation measurement for transmission tower based on close-range photogrammetry", Measurement, vol. 44, **(2011)**, pp. 1705-1712.
[17] M. Lopez, L. F. Kahn and K. E. Kurtis, "Characterization of elastic and time-dependent deformations in high performance lightweight concrete by image analysis", Cement and Concrete Research, vol. 39, **(2009)**, pp. 610-619.
[18] S. Sun, S. Yang and L. Zhao, "Noncooperative Bovine Iris Recognition via SIFT", Neurocomputing, **(2013)**, pp. 310-317.
[19] A. A. Fathima, R. Karthik and V. Vaidehi, "Image Stitching with Combined Moment Invariants and Sift Features", Procedia Computer Science, vol. 19, **(2013)**, pp. 420-427.
[20] T.-W. R. Lo and J. P. Siebert, "Local feature extraction and matching on range images: 2.5D SIFT", Computer Vision and Image Understanding, vol. 113, **(2009)**, pp. 1235-1250.
[21] Y. Li, Y. Wang, W. Huang and Z. Zhang, "Automatic image stitching using SIFT", presented at the Audio, Language and Image Processing, 2008. ICALIP 2008. International Conference, **(2008)**.
[22] B. Yu, L. Wang and Z. Niu, "A novel algorithm in buildings/shadow detection based on Harris detector", Optik - International Journal for Light and Electron Optics, vol. 125, **(2014)**, pp. 741-744.
[23] X. Zhang and X. H. Ji, "An Improved Harris Corner Detection Algorithm for Noised Images", Advanced Materials Research, vol. 433, **(2012)**, pp. 6151-6156.
[24] J. W. Hsieh, "Fast stitching algorithm for moving object detection and mosaic construction", Image and Vision Computing, vol. 22, **(2004)**, pp. 291-306.
[25] K. Chaiyasarn, T.-K. Kim, F. Viola, R. Cipolla and K. Soga, "IMAGE MOSAICING VIA QUADRIC SURFACE ESTIMATION WITH PRIORS FOR TUNNEL INSPECTION", presented at the Image Processing (ICIP), 2009 16th IEEE International Conference on, **(2009)**.
[26] G. Xu and J. Cai, "The Research of Granular Computing Applied in Image Mosaic", presented at the Informatics in Control, Automation and Robotics, 2009. CAR '09. International Asia Conference on **(2009)**.
[27] A. Elibol, N. Gracias and R. Garcia, "Fast topology estimation for image mosaicing using adaptive information thresholding", Robotics and Autonomous Systems, **(2012)**.
[28] Z. Falomir, L. Museros, L. G. Abril and F. Velasco, "Measures of similarity between qualitative descriptions of shape, colour and size applied to mosaic assembling", Journal of Visual Communication and Image Representation, vol. 24, **(2013)** pp. 388-396.
[29] J. Dou and J. Li, "Image matching based local Delaunay triangulation and affine invariant geometric constraint", Optik - International Journal for Light and Electron Optics, vol. 125, **(2014)**, pp. 526-531.
[30] Y. Zou, F. Dong, B. Lei, L. Fang and S. Sun, "Image thresholding based on template matching with arctangent Hausdorff distance measure", Optics and Lasers in Engineering, vol. 51, **(2013)**, pp. 600-609.
[31] S. Yahiaoui, M. Haddad, B. Effantin and H. Kheddouci, "Coloring based approach for matching unrooted and/or unordered trees," Pattern Recognition Letters, vol. 34, **(2013)**, pp. 686-695.
[32] U. Kang, M. Hebert and S. Park, "Fast and scalable approximate spectral graph matching for correspondence problems", Information Sciences, vol. 220, **(2013)**, pp. 306-318.
[33] C. Je and H. M. Park, "Optimized hierarchical block matching for fast and accurate image registration", Signal Processing: Image Communication, vol. 28, **(2013)**, pp. 779-791.
[34] G. Yongfang, Y. Ming and S. Yicai, "Study on an Improved Robust Algorithm for Feature Point Matching", Physics Procedia, vol. 33, **(2012)**, pp. 1810-1816.
[35] L. Cheng, M. Li, Y. Liu, W. Cai, Y. Chen and K. Yang, "Remote sensing image matching by integrating affine invariant feature extraction and RANSAC", Computers & Electrical Engineering, vol. 38, **(2012)**, pp. 1023-1032.
[36] Q. Zheng, E. Dong, Z. Cao, W. Sun and Z. Li, "Active contour model driven by linear speed function for local segmentation with robust initialization and applications in MR brain images", Signal Processing, vol. 97, **(2014)**, pp. 117-133.

[37] Q. ZHENG and E.-Q. DONG, "Narrow Band Active Contour Model for Local Segmentation of Medical and Texture Images", Acta Astronautica Sinica, vol. 39, **(2013)**, pp. 21-30.
[38] X. Xie, J. Wu and M. Jing, "Fast Two-Stage Segmentation via Non-Local Active Contours in Multiscale Texture Feature Space", Pattern Recognition Letters, vol. 34, **(2013)**, pp. 1230-1239.
[39] L. Wang, C. Li, Q. Sun, D. Xia and C.-Y. Kao, "Active contours driven by local and global intensity fitting energy with application to brain MR image segmentation", Computerized medical imaging and graphics, vol. 33, no. 7 , **(2009)**, pp. 520-531.
[40] T. F. Chan and L. A. Vese, "Active contours without edges", Image Processing, IEEE Transactions on vol. 10, **(2001)**, pp. 266-277.
[41] C. Li, C.-Y. Kao, J. C. Gore and Z. Ding, "Implicit Active Contours Driven by Local Binary Fitting Energy", presented at the 2007 IEEE Conference on Computer Vision and Pattern Recognition, Minneapolis, MN, USA, **(2007)** June 17-22.

Authors

Bo Cai, received his B.S. degree in mechatronics from China Agricultural University, in 1998, and M.S degree in Beijing University of Posts and Telecommunications, in 2003. Currently, he is the Ph.D candidate of China Academy of Engineering Physics. His research interests include image processing and detection.

Zhigui Liu, received the Ph.D degree in traffic information engineering and control from Southwest Jiao Tong University, China, in 2006. Currently, he is the teacher of Southwest University of Science & Technology, and Ph. D tutor of China Academy of Engineering Physics. His research interests include vision sensor technology, image processing and machine vision, *etc*.

Junbo Wang, received his B.S. degree in physics from Sichuan Normal University, China, in 1981, and the Ph.D degree in optical engineering from Chengdu electronic science and technology University, China, in 1985. Currently, he is the teacher of Southwest University of Science & Technology, and Ph. D tutor of China Academy of Engineering Physics. His research interests include atmospheric optical and detection, *etc*.

Yuyu Zhu, received his B.S. degree in automation from Southwest University of Science & Technology, in 2002, and M.S degree in control engineering and control theory, in 2009. Currently, he is the teacher of Southwest University of Science & Technology. His research interests include signal detection and processing, power designing *etc*.

